Received: 12 March 2018 | Revised: 11 December 2018 | Accepted: 12 March 2019

DOI: 10.4218/etrij.2018-0088

ORIGINAL ARTICLE

WILEY ETRI Journal

Numerical and experimental assessments of focused microwave thermotherapy system at 925 MHz

Jang-Yeol Kim | **Kwang-Jae Lee** | **Bo-Ra Kim** | **Soon-Ik Jeon** | **Seong-Ho Son***

Broadcasting & Media Research Laboratory, Electronics and Telecommunications Research Institute, Daejeon, Rep. Korea

Correspondence
Seong-Ho Son, Department of Mechanical Engineering, Soonchunhyang University, Asan, Rep. of Korea.
Email: son@sch.ac.kr

Present address
*Department of Mechanical Engineering, Soonchunhyang University, Asan, Rep. of Korea

Funding information
This work was supported by an Electronics and Telecommunications Research Institute (ETRI) grant funded by the Korean government [18ZR1230, Research on Beam Focusing Algorithm for Microwave Treatment] and, thanks to ZMT for a donation until November 2017 of Sim4Life used in this research.

This work investigated three-dimensional (3D) focused microwave thermotherapy (FMT) at 925 MHz for a human tissue mimicking phantom using the time reversal (TR) principle for musculoskeletal disorders. We verified the proposed TR algorithm by evaluating the possibility of 3D beam focusing through simulations and experiments. The simulation, along with the electromagnetic and thermal analyses of the human tissue mimicking phantom model, was conducted by employing the Sim4Life commercial tool. Experimental validation was conducted on the developed FMT system using a fabricated human tissue mimicking phantom. A truncated threshold method was proposed to reduce the unwanted hot spots in a normal tissue region, wherein a beam was appropriately focused on a target position. The validation results of the simulation and experiments obtained by utilizing the proposed TR algorithm were shown to be acceptable. Effective beam focusing at the desired position of the phantom could be achieved.

KEYWORDS
beam focusing, microwave thermal therapy, musculoskeletal disorder, Sim4Life, time reversal

1 | INTRODUCTION

Various modality therapies have been used for cancer treatment in recent years. The application of thermal therapies to the treatment of a variety of diseases is increasing [1]. In particular, microwave thermotherapy is known to destroy cancer cells without added side effects, and it can have a synergistic effect in combination with other therapies such as radiation therapy and chemotherapy [2]. Microwave thermotherapy ultimately aims at elevating the temperature at a tumor location to a moderate value of more than 42 °C for a sufficient period while maintaining normal temperatures in healthy tissue [3]. The focused microwave thermotherapy (FMT) technique can be useful for pain relief and the treatment of pathologies in numerous types of musculoskeletal diseases including arthritis, cancer, and inflammation. The thermal effects of such a technique on the ablation of cancer cells are currently being investigated by several groups [4–15].

In previous studies [6,9], we applied a noninvasive microwave thermotherapy method for the pathological treatment of a two-dimensional (2D) knee model using a modified time reversal (TR) algorithm. The results confirmed that a beam could be focused on a desired target position. We expanded this research to a three-dimensional (3D) environment to conduct an advanced study, the results of which are described in this article.

As preliminary research prior to investigating the FMT method using a 3D anatomical phantom model, we applied a simple 3D cylinder phantom model that mimicked muscle tissue and accounted for a large proportion of leg tissue. The simulation was conducted by utilizing Sim4Life [16], which is a finite-difference time-domain (FDTD)-based commercial tool. In addition, electromagnetic (EM) and thermal analyses

were performed at 925 MHz. We validated the possibility of effective beam focusing for a 3D muscle-mimicking phantom model in a 3D environment by considering a practical array antenna structure.

The algorithm used to focus microwave energy inside a muscle-mimicking phantom applies the TR principle [17] as a basic method. We applied a modified TR algorithm with amplitude compensation. This TR algorithm is widely used in medical imaging and therapy [13,14,17–19]. Microwave thermotherapy techniques based on the TR principle are currently being investigated for the treatment of tumors, such as those found in the breast [5,14], neck [14], and brain [20,21]. When the basic TR principle is applied to microwave thermotherapy in human tissue, the problem of unwanted hot spots may occur in normal tissue, excluding the tumor tissue in a lossy or dispersive medium. Thus, several methods [20–22] have been proposed to reduce unwanted hot spots in normal tissue in a 2D environment.

We proposed a simple method that differs from the above-mentioned methods. The proposed method, referred to as a truncated threshold method, is based on modifying the thresholds of the amplitudes calculated by employing the modified TR algorithm with amplitude compensation. The effect of the proposed method is similar to that of other conventional methods [20–22]. The method is also applicable to a 3D environment. In a previously reported study [6,9], we verified the proposed method in a 2D environment by comparing it with an existing method developed by Iero and others [20].

In addition, we experimentally validated simulation results on a 3D muscle-mimicking phantom model by utilizing the modified TR algorithm applied using the truncated threshold method in the developed FMT system.

The remainder of this paper is structured as follows: In Section 2, we describe the proposed theory on microwave thermotherapy. The computational procedures used for the microwave thermotherapy of a muscle-mimicking phantom model are described in Section 3. The numerical assessment and results are analyzed in Section 4. The experimental validation of the simulation results of the proposed phantom model is described in Section 5. Finally, concluding remarks are provided in Section 6.

2 | THEORETICAL BACKGROUND

In this section, we discuss the basic principle of the TR algorithm, the focal spot size used for EM analysis, and the Pennes equation of bioheat transfer for thermal analysis.

2.1 | EM analysis using the TR method

The TR principle [17] exploits the invariance of the wave equation under TR. This governing wave equation ensures that, for every wave diverging away from a source, there exists a reverse wave that precisely retraces the path of the original wave back to the source. This occurs regardless of the presence of scattering objects or inhomogeneities in permeability and permittivity. The reverse wave converges and focuses coherently at the original source location as if moving back in time, $t \to -t$.

However, the TR principle in a lossy medium has certain challenges such as the occurrence of unwanted hot spots at a nontarget position and the difficulty in beam focusing at a target position. To solve this problem, we consider a modified TR method with amplitude compensation for computing the wave propagation between a target point and receiver points for a sinusoidal signal with a time-varying field. This equation can be expressed as a phasor notation with time and space to solve the TR propagation. The incident field at the target position at r can be written as

$$E(r,t)_{\text{inc}} = E_0 e^{-\alpha r} e^{-j\beta r} e^{-j\phi} e^{j\omega t}, \tag{1}$$

where E_0 is the amplitude of the electric field, α is the attenuation constant, and β *i*s the phase constant. The incident field, which is an initial source located at the target position at, propagates the receiver position at r_1 in the forward step of the TR. In the reverse step of the TR, the received field at r_1 is used as the source to transmit in the TR order. The electric field, $E(d,t)$, at distance d ($r_1 = d$) can be represented by

$$E(d,t) = E_0 e^{-\alpha d} e^{-j\beta d} e^{-j\phi}. \tag{2}$$

$E(d,t)$ is equal to $E(r_1,t)$. Here, $E(d,t)$ can be expressed in the polar form as follows:

$$\left(\log_{10} E_0 - \alpha d \times 10\log_{10} e\right) \angle(-\beta d - \phi), \tag{3}$$

$$(E_0 - m)\angle(-\beta d - \phi), \tag{4}$$

where m is the attenuation amount (given by α) between the target position at r and the receiver position at d. The electric field is returned to the target position. Compared with the incident field, the amplitude of the electric field is attenuated and its phase is reversed. In other words, if the electric field at the receiver position is returned to the target position, the attenuation in amplitude increases by the amount of attenuation and the phase is reversed to obtain the original phase at the target position. Accordingly, the relationship between the TR electric field, $E(d,t)_{\text{TR}}$, and the electric field, $E(d,t)$, at the receiver position is as follows:

$$\frac{|E(d,t)_{\text{TR}}|}{|E(d,t)|} = \frac{e^{+\alpha d}}{e^{-\alpha d}} = e^{2\alpha d} = 2\alpha d \times 10\log_{10} e = 2m. \tag{5}$$

The receiver position becomes the new original position as a transmit position. The initial values of the TR electric field, $E(0,t)_{\text{TR}}$, can be written as

$$E(0,t)_{\text{TR}} = (E_0 + m)\angle(\beta d + \phi), \tag{6}$$

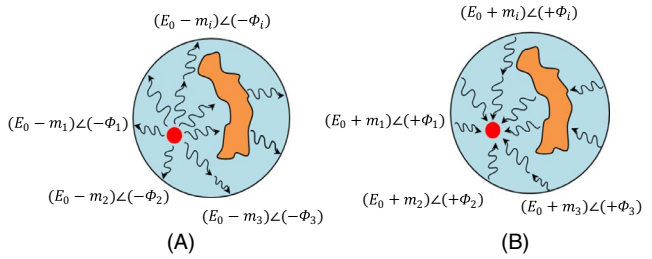

FIGURE 1 Modified TR method with amplitude: (A) Forward and (B) reverse TR steps

where $E(0,t)_{\mathrm{TR}}$ is equal to $E(r_1,t)_{\mathrm{TR}}$. The TR electric field, $E(r_1,t)_{\mathrm{TR}}$, can be expressed as

$$E(r_1,t)_{\mathrm{TR}} = E_0 e^{-\alpha r} e^{\alpha r_1} e^{-j\beta r} e^{j(\beta r_1+\phi)} e^{j\omega t}. \tag{7}$$

Furthermore, the amplitude of the returned TR electric field is the maximum, with the same phase as that at the target position.

Figure 1 shows the proposed modified TR method with the amplitude for the focusing of the target position in an inhomogeneous medium. Figure 1A illustrates the forward step for the propagation of an incident field with an input continuous wave (CW) signal. A point source located at the target position of the inhomogeneous medium transmits the CW signal. The transmitted signal propagates in the inhomogeneous medium, and it is received by an n-element antenna array to obtain amplitude and phase data. Figure 1B illustrates the reverse step for the backward propagation of the time-reversed CW signal. The initial transmitter at the target position is removed in the reverse step. The received signal in each array element contains information on amplitude and phase. Each element array turns into a transmitter for the focusing of the target position. This element array, with the amplitude and phase calculated using the proposed TR algorithm, propagates at the initial target position.

A power absorption distribution (PAD) is used as the heat source for thermal analysis. PAD values indicate the amount of power absorbed in tissue generated by the electric field in EM analysis, and they are given by

$$\mathrm{PAD} = \frac{\sigma}{2} E^2 \tag{8}$$

where σ is the electrical conductivity and E^2 is the square of the magnitude of the electric field. PAD values differ from the specific absorption rate (SAR) only in terms of tissue density.

In addition, the wavelength (λ_g) for the calculation of focal spot size (δ) can be expressed as

$$\lambda_g = \frac{c}{f\sqrt{\varepsilon_{\mathrm{r}}}}, \tag{9}$$

where c is the speed of light, f is the operating frequency, and ε_{r} is the relative dielectric permittivity. Here, the focal spot size (δ) is defined as the diffraction limit, which is represented as 0.5 λ_g. The focal spot size (δ) can be approximated using 0.5 λ_g. This focal size represents the electrical length, and the time interval (Δt) is not considered.

2.2 | Temperature Analysis

A temperature profile is used to determine the effective thermal phenomena for the muscle-mimicking phantom model. This equation is the well-known the Pennes bioheat equation [4,5], and it can be written as

$$C \cdot \rho \cdot \frac{\partial T}{\partial t} = \nabla \cdot (K \cdot \nabla T) + A_0 + \rho \cdot SAR - B \cdot (T - T_{\mathrm{B}}) \tag{10}$$

where C is the specific heat, ρ is the tissue density, K is the thermal conductivity, A_0 is the metabolic heat production. $\rho \cdot SAR$ is equal to Q, and it is the heating potential of the heat source. In addition, Q is the same as the PAD, and it can be computed by utilizing the FDTD-based EM solver through (8). Here, B is the capillary blood perfusion coefficient, T is the temperature, and T_{B} is the temperature of blood. The detailed thermal parameters associated with (10) depend on the tissue type. Additionally, when heat duration is short, (10) can be re-expressed for the increase in tissue temperature (ΔT) and the time interval (Δt). The increase in tissue temperature is given by

$$\Delta T = \frac{1}{C} \mathrm{SAR} \Delta t, \tag{11}$$

where C is the specific heat of the tissue. The metabolic heat production, thermal conductivity, and capillary blood perfusion coefficient are neglected. Table 1 lists the typical average values of the thermal properties of the tissue of a muscle thermal model [23] and the muscle-mimicking thermal phantom. The thermal properties of the muscle-mimicking thermal phantom model were obtained through measurement devices.

3 | COMPUTATIONAL PROCEDURE

The proposed computational procedure for the FMT of the muscle-mimicking phantom model using the EM theory with the TR algorithm and the thermal theory with the bioheat equation is shown in Figure 2. We constructed an EM model of a 3D cylinder muscle-mimicking phantom and a 3D thermal model by employing Sim4Life. This model, which was composed of homogeneous tissue, was mapped to the permittivity, conductivity, and thermal properties.

TABLE 1 Thermal properties of the tissue

Tissue	Specific heat C (J/kg°C)	Tissue density ρ (kg/m^3)	Thermal conductivity K (W/m°C)	Metabolic heat production A_0 (W/m^3)	Capillary blood perfusion B (W/m^3°C)
Muscle	3421	1090	0.495	906	2706
Muscle-mimicking phantom	1019	1151	0.536	0	0

The forward step of the EM TR was applied to acquire received signal data with amplitude and phase from the signal transmitted to the target position using the muscle-mimicking phantom model in the simulation software.

The truncated threshold method was applied by utilizing the amplitude values obtained from the forward step of the EM TR. This method can reduce unwanted hot spots in a normal tissue area, and it uses an amplitude value below the threshold. The determination of the threshold for the proposed method is shown in Figure 2. When the acquired amplitude values were normalized, the threshold was assumed to be 1. This threshold is the initial value.

Next, the reverse step of the EM TR was applied for the beam focusing at the target position. To apply this step, the receiver position with the receiver array antennas was changed to the transmit position using the array as the transmission antennas.

As a result of this reverse step, PAD data (ie, heating potential Q) were obtained for thermal analysis.

The thermal analysis was performed after the EM analysis was completed. As a preliminary step of the thermal analysis, a mapping of the dedicated thermal model of the muscle-mimicking phantom was applied, the thermal parameters were generated, and the heat source was confirmed. Then, FDTD thermal simulation was carried out.

The thermal analysis confirmed that the temperature at the target position reached 43 °C and that the temperature of the normal surrounding tissue was below 42 °C. When the temperature of the tumor was below 43 °C, the temperature of the normal surrounding tissue was verified to confirm whether unwanted hot spots occurred above 42 °C. When unwanted hot spots occurred, the threshold of the amplitude used to obtain the new thermal analysis results was updated. The appropriate threshold was replaced by $\text{threshold}_{\text{new}}$. Here, the value of Δstep used to calculate $\text{threshold}_{\text{new}}$ was 0.1. The reverse step of the EM TR and the thermal analysis were re-applied to reduce damage to the normal surrounding tissue using the appropriately selected threshold.

When the temperature at the target position was above 43 °C, the temperature of the normal surrounding tissue was verified. The thermal analysis was completed when unwanted hot spots stopped occurring in the surrounding normal tissue.

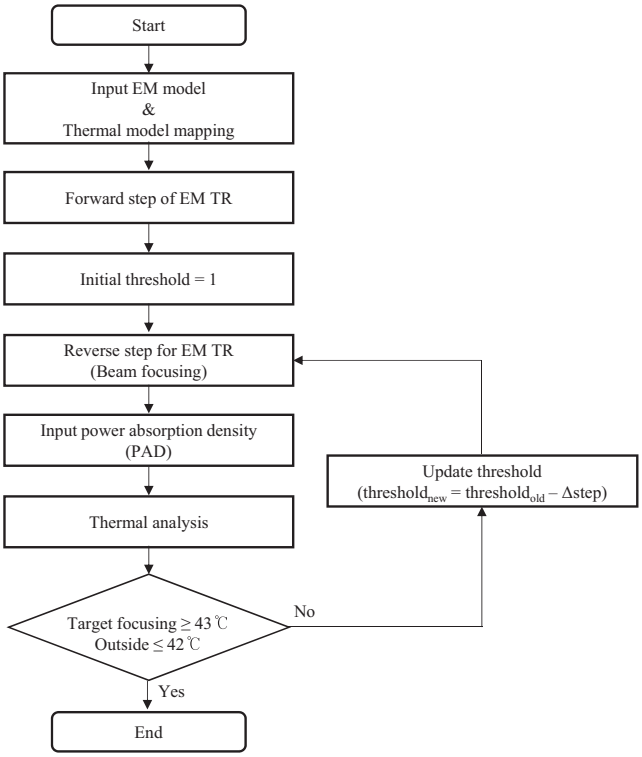

FIGURE 2 Flowchart of the proposed focused microwave thermotherapy method

4 | NUMERICAL ASSESSMENT

We used beam focusing at the target position of the 3D muscle-mimicking phantom model to verify the effectiveness of the proposed TR algorithm in a 3D environment. EM and thermal simulations were conducted using Sim4Life at 925 MHz.

4.1 | EM analysis

Figure 3 shows the design of the muscle-mimicking phantom model for the forward step of the EM TR. This model was mapped using permittivity ($\varepsilon_r = 55$) and conductivity ($\sigma = 0.5$ S/m) that were similar to those of normal muscle tissue ($\varepsilon_r = 55$, $\sigma = 0.95$ S/m). We considered the target position of the phantom to obtain signal data with amplitude

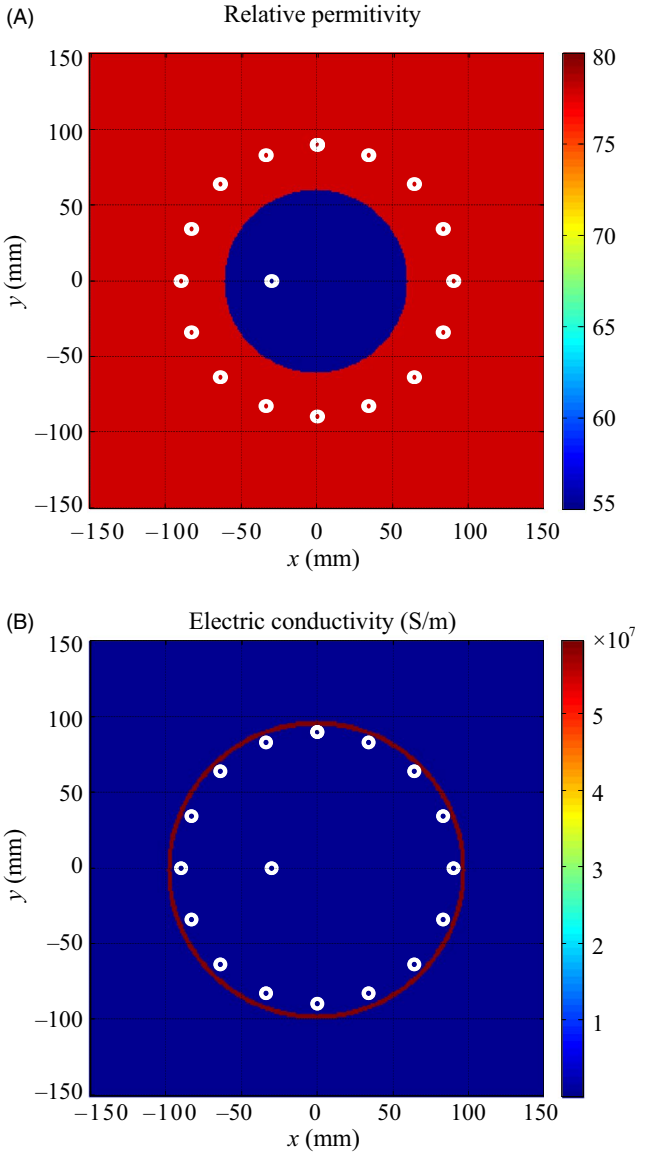

FIGURE 3 Muscle-mimicking phantom model for the forward step of the EM TR in an environment mapped with (A) permittivity and (B) conductivity

and phase. The target was offset to the left (x: −30 mm; y: 0 mm) from the center (x: 0 mm; y: 0 mm) of the model. A transmission antenna with an input CW source was located at the target position. A 16-receiver antenna array with a circular configuration was located outside the model. The receiver antennas with an array diameter of 180 mm were located in the background medium (distilled water with $\varepsilon_r = 78$ and $\sigma = 0.2$ S/m). The back of the receiver antennas was implemented in the circular metal boundary as a cavity structure. The total area of the simulation was 300 × 300 mm^2. The mesh cell size was 1 mm. FDTD-based 2D EM simulation was conducted in the developed EM solver to obtain the amplitude and phase data at the 16-receiver array antenna position until a steady state condition was reached. The main reasons for using 2D simulation in the forward step of the EM TR are as follows: First, the calculated signal data can confirm that the 2D and 3D simulation results are similar, as shown in Figure 4B. Second, 2D simulation for approximately 1.5 minutes can be used to rapidly acquire signal data with amplitude and phase at the 16-receiver position, whereas 3D simulation requires approximately 6 hours for the forward step of the EM TR. Third, a 2D EM forward solver is applied to the developed FMT system for the beam-focusing experiment. Currently, a 3D EM forward solver is being developed owing to the difficulty in constructing the environment of a commercial tool for 3D analysis in the FMT system. Ultimately, the developed 3D EM solver will be applied to the FMT system. For this study, Sim4Life was provided by Zurich MedTech (Switzerland) for a certain period. Thus, the forward analysis of the EM TR for obtaining amplitude and phase data was effectively conducted using 2D simulation.

Figure 4A shows the results for the forward step of the EM TR used to obtain amplitude and phase data. The graph shows the acquired amplitude and phase data for the muscle-mimicking phantom model at the 16-receiver array antenna position. Herein, we propose a truncated threshold method to reduce the unwanted hot spots in a normal tissue area excluding the target position.

This method involves the adjustment of the threshold for the amplitude values of the 16-array antennas. When

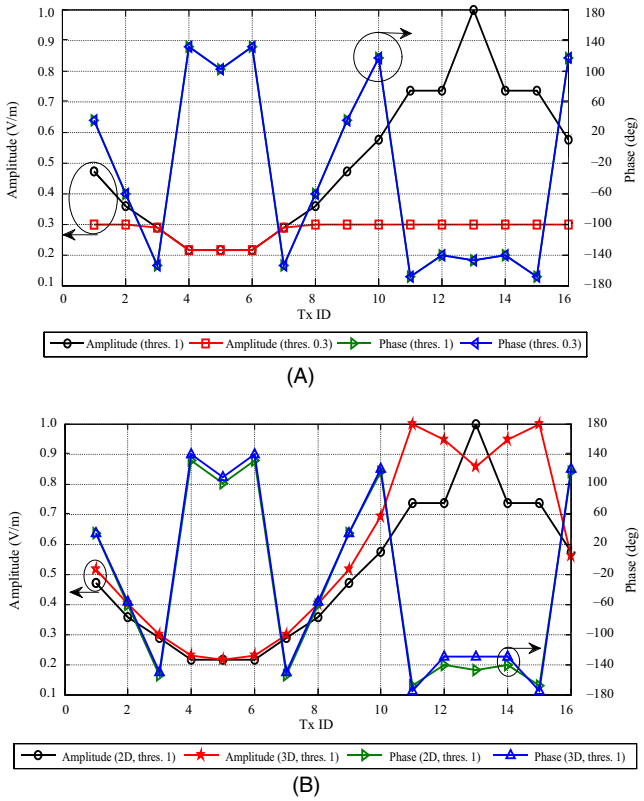

FIGURE 4 Calculation results of the amplitude and phase in the phantom model: (A) 2D environment for the truncated threshold method, and (B) comparison of the results in 2D and 3D environments

the amplitude values were normalized, the threshold was assumed to be 1. Figure 2 details this method, which uses an amplitude value below the threshold. The truncated threshold was applied to the muscle-mimicking phantom model.

Figure 4B shows the amplitude and phase data acquired in the 2D and 3D simulations, the results of which are confirmed to be similar. The results for the amplitude data for a few transmit antennas are different when considering a practical 3D array antenna structure and when using a 2D point source; this is the cause of the limitation of a 2D simulation. If the truncated threshold method is applied for unwanted hot-spot control in a normal tissue region, the results of the 2D and 3D amplitude data are the same (eg, for a threshold of 0.3).

In contrast, the results of the 2D and 3D phase data are almost the same. These abovementioned results confirm that the 2D simulation used to obtain signal data can obtain results similar to those of the 3D simulation.

To analyze the reverse step and determine the effects of unwanted hot spots in the normal tissue area of the muscle-mimicking phantom model, the design shown in Figure 5 was applied. The receiver array antennas employed in the forward step were converted into transmission array antennas in the reverse step, and the initial transmission antenna located at the target position was removed. This model type was a 3D cylindrical phantom model with a diameter of 120 mm and a height of 250 mm, and it was located inside the practical array antenna structure. These array antennas were included in a cylindrical metal cavity structure that served as an illumination tank. The proposed antenna type, which is shown in Figure 5A, was the directional dipole structure on the Taconic CER-10 substrate with a dielectric constant of 10. This antenna was coupled to the circular waveguide metal structure, as shown in Figure 5A. The proposed antenna was extended to 16-array antennas with a metal cavity structure, as shown in Figure 5B. Thus, the reverse step simulation of the EM TR using the 16-array antennas was effectively applied, as shown in Figure 5C. The area between the phantom model and array antennas was filled with distilled water ($\varepsilon_r = 78$, $\sigma = 0.2$ S/m).

The reverse step of the EM TR in a 3D environment was conducted using the calculated amplitude and phase data, as shown in Figure 4A. Figure 6 shows the results of the application of the reverse step of the EM TR.

Figure 6A–6C show the PAD results of the 3D muscle-mimicking phantom model for a threshold of 1. The PAD values are at their maximum at the right edge position of the phantom model but not for the target position on the left side. Under this condition, unwanted hot spots are observed at the edge area on the right. This is a major problem that should be resolved to effectively focus the beam at the target position.

The amplitude threshold values were adjusted to reduce unwanted hot spots at the right edge position of the phantom model. Figure 6D–6F show the PAD results for threshold of 0.3 obtained using the threshold determination method shown in Figure 2. The PAD value is at its maximum at the

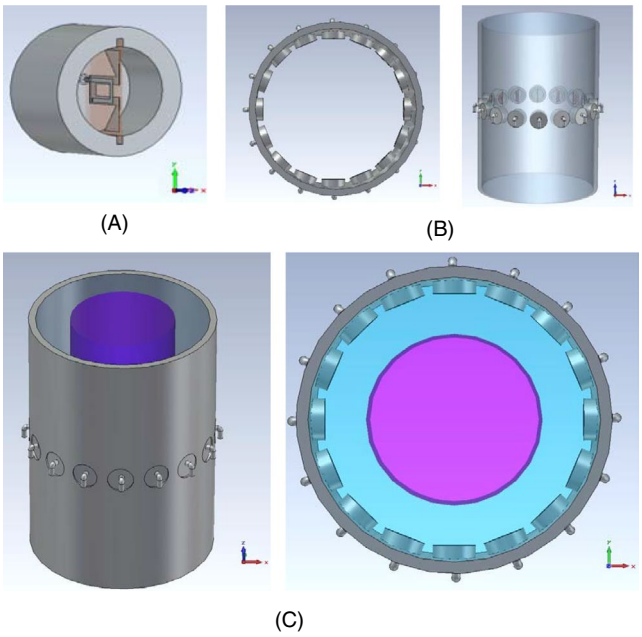

FIGURE 5 Design of the reverse step of the EM TR for the (A) proposed antenna, (B) 16-array structure with an illumination tank, and (C) 16-array antenna structure with an illumination tank and a 3D cylindrical phantom model

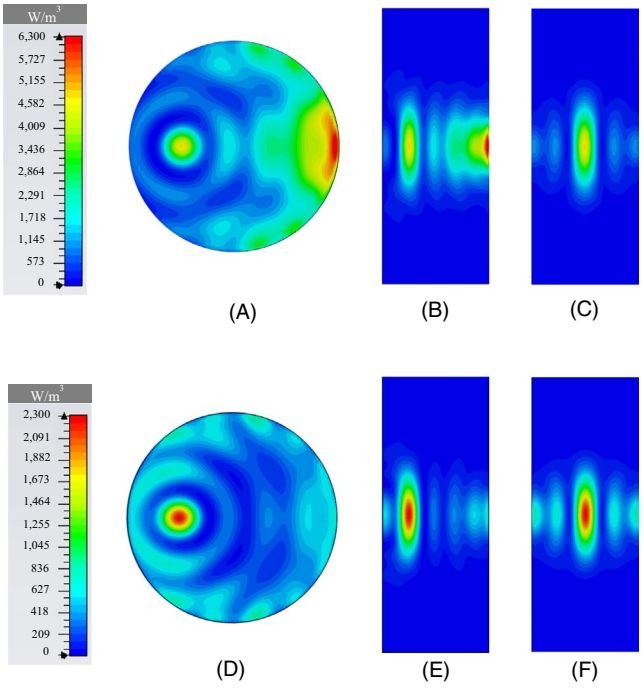

FIGURE 6 Results of PAD in the phantom model in the (A) *x-y* plane, (B) *x-z* plane, and (C) *y-z* plane with a threshold of 1, and in the (D) *x-y* plane, (E) *x-z* plane, and (F) *y-z* plane with a threshold of 0.3

target position of the phantom model compared to the other normal tissue areas. In addition, effective beam focusing is achieved at the target position, thus reducing the occurrences of unwanted hot spots at the left edge position of the phantom model. Therefore, the accuracy of the proposed TR algorithm is confirmed.

The focal spot size of the phantom model, as shown in Figure 6, can be calculated using (9). As the permittivity of the phantom model is 55 based on (9), the theoretical focal size is calculated as 22 mm, corresponding to 0.5 λ_g. The focal spot size according to the simulation results in Figure 6 is 21 mm, which corresponds to 0.48 λ_g compared to the theoretical result. The theoretical and simulated focal spot sizes are almost the same. The focal spot sizes shown in Figure 6A–6C and 6D–6F are the same. Regardless of the threshold value, the wavelength of the phantom model does not change, and thus, the focal spot size is the same. The theoretical and simulation results meet the diffraction limit, and the focal spot size in the EM analysis corresponds to approximately 0.5 λ_g.

4.2 | Thermal analysis

The thermal analysis of the muscle-mimicking phantom model was conducted using the FDTD-based Sim4Life software and bioheat equation. We constructed a 3D thermal model by mapping the thermal properties of the tissue, as listed in Table 1. The PAD data were used as the heat source. We applied two thermal simulations to confirm the beam focusing possibility of the proposed TR algorithm. For the first thermal simulation of the muscle-mimicking thermal model, the temperature of the background medium was set as 15 °C with a convection coefficient of 300 W/m^{2}K [4]. The initial temperature of the model was assumed to be 37 °C, which is the same as the temperature of the human body. The second thermal simulation was conducted considering the thermal properties of the muscle-mimicking phantom model, as listed in Table 1. This simulation was applied to compare the experimental validation results achieved using the fabricated muscle-mimicking phantom model. Thus, the conditions of the thermal simulation were set to be the same as those of the experiment. The temperature of the background medium was set as 19 °C with a convection coefficient of 300 W/m^{2}K. The initial temperature of the muscle-mimicking thermal model was assumed to be 19 °C. In addition, while conducting the thermal analysis using PAD data in the two simulations, the authors checked whether an unwanted hot spot occurred in the surrounding normal tissue when the target-position temperature of the proposed model reached 43 °C.

The first simulation provides the thermal-analysis results for the muscle-mimicking thermal model with mapped thermal properties for the muscle tissue, as listed in Table 1. Figure 7 shows the thermal-analysis results for the muscle-mimicking thermal model during a 10-min period. As indicated by the PAD results in Figure 6A–6C, with an applied threshold of 1, the results of the thermal analysis shown in Figure 7A–7C are poor. The temperature increases from 37 °C to 44.9 °C, and unwanted hot spots appear in normal tissue areas such as close to the right edge area. When using an input power of 42.5 W, the temperature at the hot spot increases to up to 44.9 °C and the temperature at the target position reaches 43 °C for a threshold of 1. To reduce unwanted hot spots close to the right edge area of the normal tissue for the thermal model, we reapplied the thermal analysis based on the PAD result with an adjusted amplitude threshold by utilizing the new truncated threshold method. Figure 7D–7F show the results of the thermal analysis obtained using the PAD results shown in Figure 6D–6F, respectively, for a threshold of 0.3. For an input power of 25 W, the temperature at the target position increases from 37 °C to 43 °C when the temperature of the surrounding normal area is below 38.8 °C. Moreover, unwanted hot spots do not occur close to the right edge area of the normal tissue.

Figure 8A shows the results of the focal spot size for the cases shown in Figure 7A–7C, for a threshold of 1. Here, the focal spot size obtained from the thermal analysis corresponds to approximately 0.25 λ_g of the electrical wavelength in (9); in addition, the time interval (Δt) in (11) is considered. That is, during the thermal analysis, the focal spot size can be obtained by considering (9) and (11). In addition, the

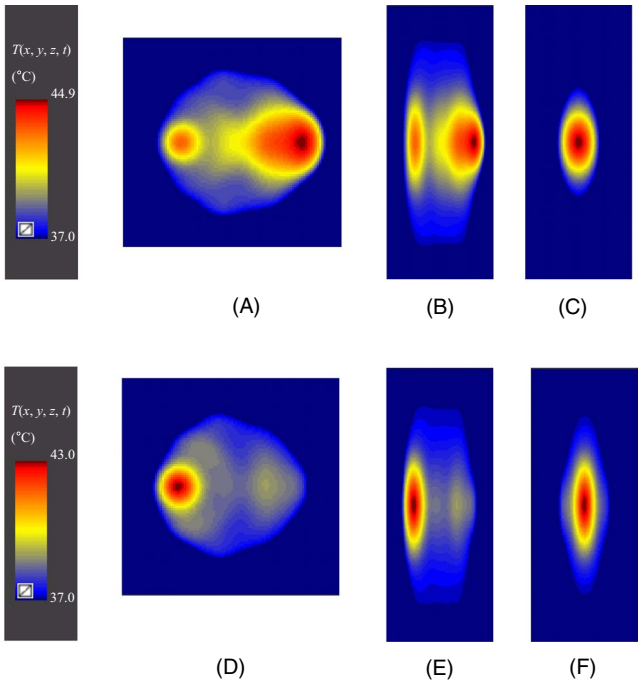

FIGURE 7 Results of thermal analysis in the muscle-mimicking thermal model in the (A) *x*-*y* plane, (B) *x*-*z* plane, and (C) *y*-*z* plane with a threshold of 1 within a temperature range of 37 °C–44.9 °C, and in the (D) *x*-*y* plane, (E) *x*-*z* plane, and (F) *y*-*z* plane with a threshold of 0.3 within a temperature range of 37 °C–43 °C

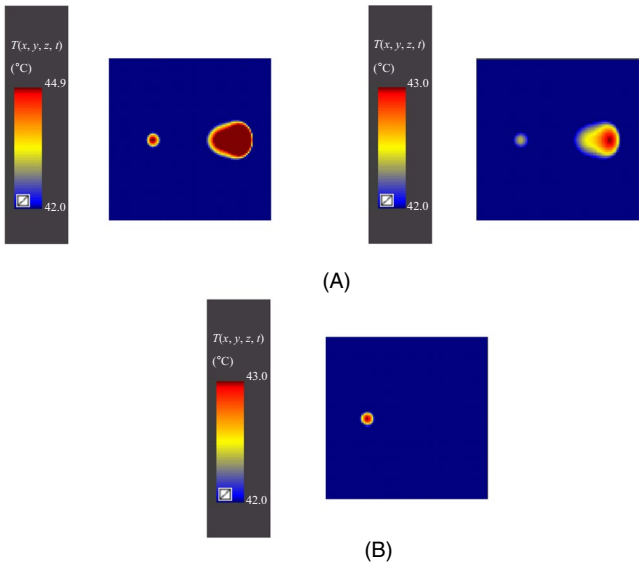

FIGURE 8 Results of the focal spot size of the thermal model for a threshold of (A) 1 and (B) 0.3

focal spot size of the model corresponding to approximately 0.25 λ_g is determined as the area when the initial temperature is increased by 5 °C. Therefore, the reference temperature employed to determine the hot spot temperature in normal tissues of the human body is 42 °C, which is the normal temperature of 37 °C increased by 5 °C. Then, therapeutic effects are observed for temperatures above 42 °C. In other words, the reference temperature of 42 °C indicates the maximum temperature that can be sustained before the normal tissue is damaged, which is a temperature corresponding to approximately 0.25 λ_g to obtain the focal spot size of the proposed phantom model. The left and right images in Figure 8A indicate a different temperature range to demonstrate the visual effects of the focal spot size. Further, the focal spot sizes of both figures are the same in the target and hot spot regions. The focal spot size is 10 mm (*x*-axis, *y*-axis) at the target position and 35 mm (*x*-axis) and 30 mm (*y*-axis) at the right edge of the hot spot region for a reference temperature of 42 °C, as shown in Figure 8A. Figure 8B shows the results of the focal spot size for the cases shown in Figure 7D–7F, for a threshold of 0.3. The focal spot size is 10 mm (*x*-axis, *y*-axis) at the target position for a reference temperature of 42 °C. The focal spot size in this simulation is 0.23 λ_g, in contrast with the theoretical result of 11 mm, which corresponds to 0.25 λ_g at the target position. The focal spot size at the target position is equal to 10 mm regardless of the threshold values, for a reference temperature of 42 °C. This is because the temperature at the target position increases equally by 6 °C (corresponding to 43 °C) according to (11).

The second simulation provides the results of the thermal analysis for the muscle-mimicking thermal model. Figure 9 shows the thermal analysis results for the model during a 10-min period. As shown in Figure 9A–9C, for a threshold

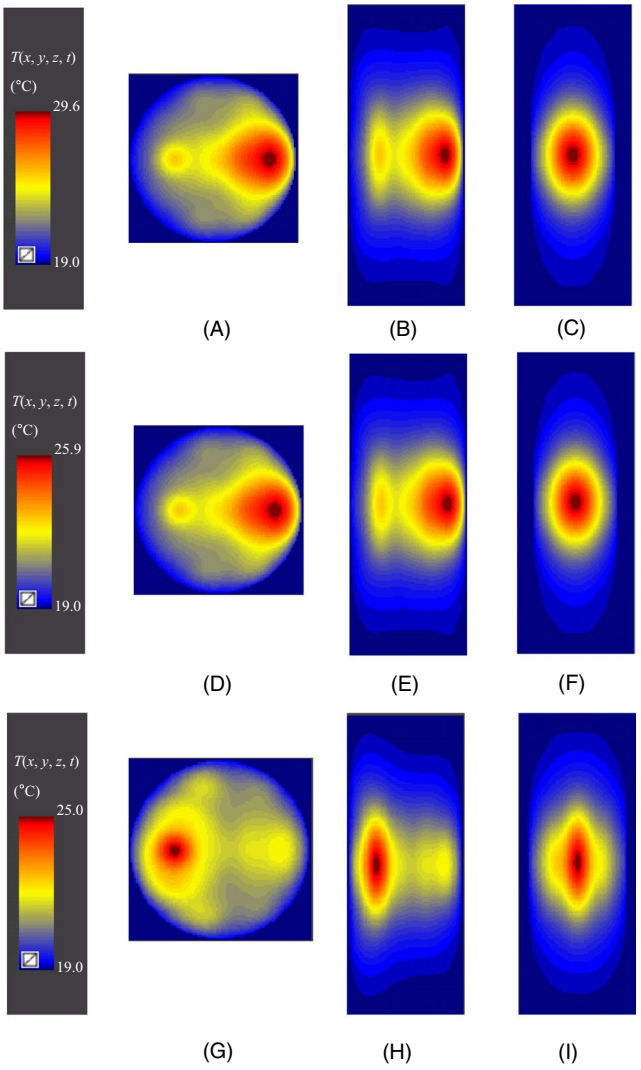

FIGURE 9 Results of thermal analysis in the muscle-mimicking thermal model in the (A) *x*-*y* plane, (B) *x*-*z* plane, and (C) *y*-*z* plane for a threshold of 1 within a temperature range of 19 °C–29.6 °C; in the (D) *x*-*y* plane, (E) *x*-*z* plane, and (F) *y*-*z* plane for a threshold of 1 within a temperature range of 19 °C–25.9 °C; in the (G) *x*-*y* plane, (H) *x*-*z* plane, and (I) *y*-*z* plane for a threshold of 0.3 within a temperature range of 19 °C–25 °C

of 1, the results of the thermal analysis are poor. The temperature increases from 19 °C to 29.6 °C, and an unwanted hot spot appears close to the right edge. For an input power of 20 W, the temperature at the target reaches 25 °C (relatively equal to 43 °C within a range of 37 °C–43 °C) and the temperature at the unwanted hot spot increases by a maximum of 29.6 °C (relatively equal to 47.6 °C within a range of 37 °C–43 °C). Figure 9D–9F show the thermal analysis results for the muscle-mimicking thermal model for a threshold of 1 for a comparison of the same temperature range with the experimental results of the phantom model at 19 °C–25.9 °C. For an input power of 13.1 W, the temperature at the target position increases from 19 °C to 25.9 °C (relatively equal

to 43.9 °C within a range of 37 °C–43 °C) and the temperature of the surrounding normal tissue area with the right edge area is 23 °C (relatively equal to 41 °C within a range of 37 °C–43 °C). Figure 9G–9I show the thermal analysis results for the muscle-mimicking thermal model for a threshold of 0.3. for an input power of 11.9 W, the temperature at the target position increases from 19 °C to 25 °C and the temperature of the surrounding normal tissue at the right edge is below 22.1 °C (relatively equal to 40.1 °C within a range of 37 °C–43 °C).

Figure 10A shows the results of the focal spot size for the cases shown in Figure 9A–9C, for a threshold of 1. The left and right images in Figure 10A indicate different temperature ranges to show the visual effect of the focal spot size. The focal spot sizes in both figures are equal in the target and hot spot regions. The focal spot size is 11 mm (*x*-axis, *y*-axis) at the target position and 57 mm (*x*-axis) and 53 mm (*y*-axis) in the hot spot region at the right edge, for a reference temperature of 24 °C (relatively equal to 42 °C within a range of 37 °C–43 °C, where $= \Delta T5$ °C). Figure 10B shows the results of the focal spot size for the cases shown in Figure 9D–9F, for a threshold of 1. The focal spot size is only 31 mm (*x*-axis) and 29 mm (*y*-axis) in the hot spot region at the right edge for a reference temperature of 24 °C. As shown in Figure 9A–9C and Figure 9D–9F, even when the threshold value is 1, it is possible to confirm that the focal spot size in the hot spot region is different because the increase in tissue temperature, (T given by (11)) in the hot spot region differs depending on input power. Figure 10C shows the result of the focal spot size for the cases shown in Figure 9G–9I, for a threshold of 0.3. The focal spot size is 11 mm (*x*-axis, *y*-axis) at the target position for a reference temperature of 24 °C. This focal spot size is the same as the theoretical result of 11 mm corresponding to 0.25 λ_g at the target position.

The focal spot size at the target position is equal to 11 mm regardless of the threshold value, for a reference temperature of 24 °C. This is because the temperature at the target position increases equally by 6 °C (corresponding to 25 °C) according to (11).

The input powers for the first and second simulations are different for the following reasons: The first reason is the difference in the thermal properties of the muscle tissue and muscle-mimicking phantom tissue listed Table 1, in particular, the difference between the metabolic heat production and capillary blood perfusion of the two models. The second reason is the difference in tissue temperature increase (ΔT) according to (11). In the two simulations, the input power required for a threshold of 1 is higher than that for a threshold of 0.3. This is because for a threshold of 1, input power increases temperature in two regions. The temperature of the hot spot region is increased by more than 6 °C and the temperature at the target position is raised by 6 °C. However, when the threshold value is 0.3, input power increases only the temperature at the target position by 6 °C. The focal spot size at the target position for the thermal model is similar for both simulation results. This is because the focal spot size is satisfied at approximately 0.25 λ_g in the thermal analysis. In conclusion, as shown by the two simulation results, the possibility of beam focusing by the proposed TR algorithm for the muscle-mimicking phantom model is confirmed.

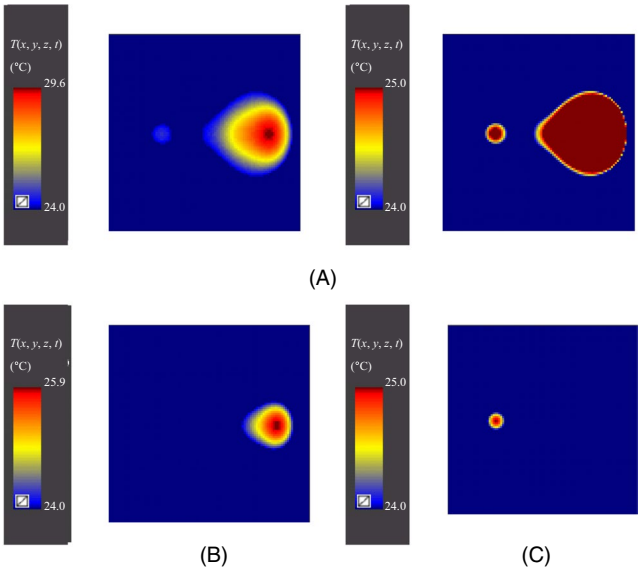

FIGURE 10 Focal spot size results of the muscle-mimicking thermal model: (A) spot size for a threshold of 1 within a temperature range of 24 °C–29.6 °C, (B) spot size for a threshold of 1 within a temperature range of 24 °C–25.9 °C, and (C) spot size for a threshold of 0.3 within a temperature range of 24 °C–25 °C

5 | EXPERIMENTAL ASSESSMENT

In this section, the simulation results of the proposed muscle-mimicking phantom model obtained using the developed FMT system are experimentally validated.

Figure 11 shows the overall block diagram and configuration of the developed FMT system. This system comprises several components used to conduct the experiment for the beam focusing of the phantom model.

The 16 transmission array antennas use a directional dipole that utilizes a 1.27-mm thick Taconic CER-10 substrate with a dielectric constant of 10. The operating frequency is 925 MHz (VSWR < 2). The illumination tank is a cylindrical metal cavity structure filled with distilled water ($\varepsilon_r = 78$, $\sigma = 0.2$ S/m) to demonstrate the cooling effect. The 16 transmission array antennas are coupled to the center part of the illumination tank, shown in Figure 11B. The cooling device circulates and cools the distilled water in the illumination tank to maintain a set temperature below 20 °C. This is configured in the circulating pump and cooling module. As shown in the block diagram of Figure 11A, the FMT transmitter

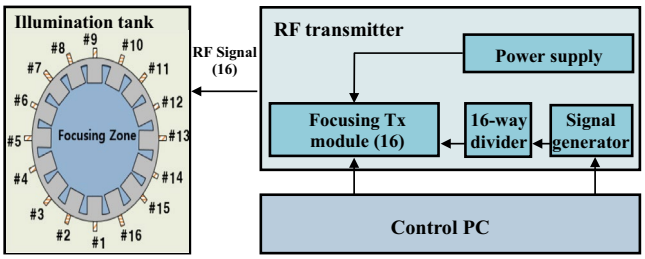

(A)

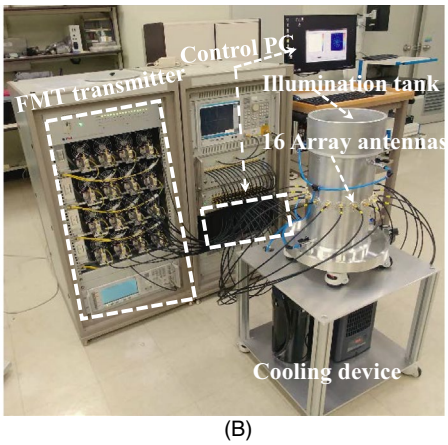

(B)

FIGURE 11 Configuration of the FMT system: (A) Overall block diagram of the FMT system and the (B) developed FMT system

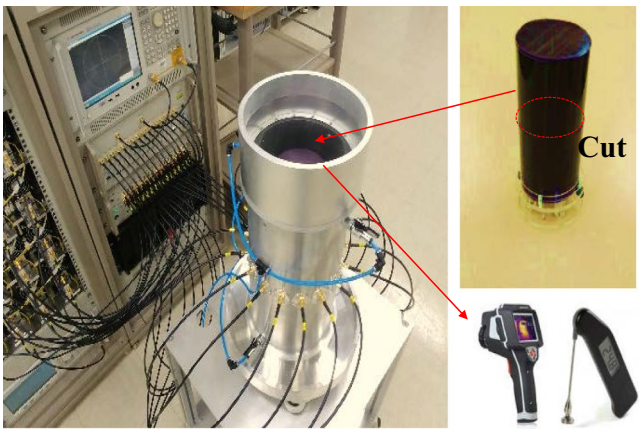

FIGURE 12 Beam focusing experiment and experimental procedure

is comprised of a signal generator (Keysight E4438C ESG Vector Signal Generator), 16-way power dividers, 16-channel Tx modules, 16-channel power amplifiers, 16-channel directional couplers, and a power supply. A control PC is used to operate the developed FMT system for experimental validation.

We manufactured a 3D cylinder-type muscle-mimicking phantom with $\varepsilon_r = 55$ and $\sigma = 0.5$ S/m. The phantom was fabricated using gelatin powder mixed with distilled water, watercolor paint, and thermochromic pigment.

For the experiment, the fabricated phantom was inserted into the illumination tank of the FMT system. The beam focusing experiment was conducted using the phantom shown in Figure 12. As a test condition, the temperature of the distilled water as the background medium was set as 19 °C using a cooling device, as was the temperature of the 3D muscle-mimicking phantom.

The power and phase values of the 16 transmission array antennas of the FMT system were applied for thresholds of 0.3 and 1, as used in the simulations described in Section IV. The signal generator of the FMT system provided a continuous signal at a frequency of 925 MHz; the applied input power was 37.5 W for a threshold of 1 and 27 W for a threshold of 0.3, for an exposure time of 10 min in the beam focusing test. For the phantom test, the phantom was truncated into two pieces, as shown in Figure 12, and the truncated portion of the phantom was wrapped with tape. Here, the input power used in the experiment was higher than that used for the simulation. To confirm the temperature results of the phantom, the phantom inserted in the illumination tank was taken out, following which it was separated into two pieces. The temperature of the focused area for one of the two truncated pieces was measured using an infrared (IR) camera. During this process, a period of several seconds elapsed and the temperature at the target position for the phantom changed. Therefore, considering the above situation, to compare the simulation and experimental results, we used a higher input power during the actual experiments compared to the simulation.

Figure 13 shows the results of the beam focusing for the phantom, which were confirmed using an IR camera and a thermometer. Figure 13A shows an image corresponding to one of the two pieces of the truncated phantom after conducting the experiment using a threshold of 1. This image confirms that an unwanted hot spot occurs in the right edge area of the phantom next to the beam focusing at the target position (x, –30 mm; y, 0 mm). As shown in Figure 13C, the temperature at the hot spot for the phantom increases up to 25.9 °C and the temperature at the target position reaches 23.2 °C. We conducted a beam focusing experiment with an applied threshold of 0.3 to reduce the unwanted hot spot close to the right edge area of the phantom. Figure 13B shows the beam focusing image corresponding to one side of the phantom when it is separated into two pieces after conducting the experiment with a threshold of 0.3. It can be confirmed that the beam focusing of the phantom occurs at the target position without any unwanted hot spots, as shown in Figure 13B. The temperature at the target position for the phantom reaches 24.8 °C, as shown in Figure 13D and 13H. The temperature at the target position for the phantom changes from 19 °C to 24.8 °C (relatively equal to 42.8 °C within a range of 37 °C–43 °C, at approximately = ΔT6 °C), whereas the temperature of the surrounding normal tissue area with the left edge area increases to up to 21.3 °C (relatively equal to 39.3 °C within a range of 37 °C–43 °C). Figure 13E shows

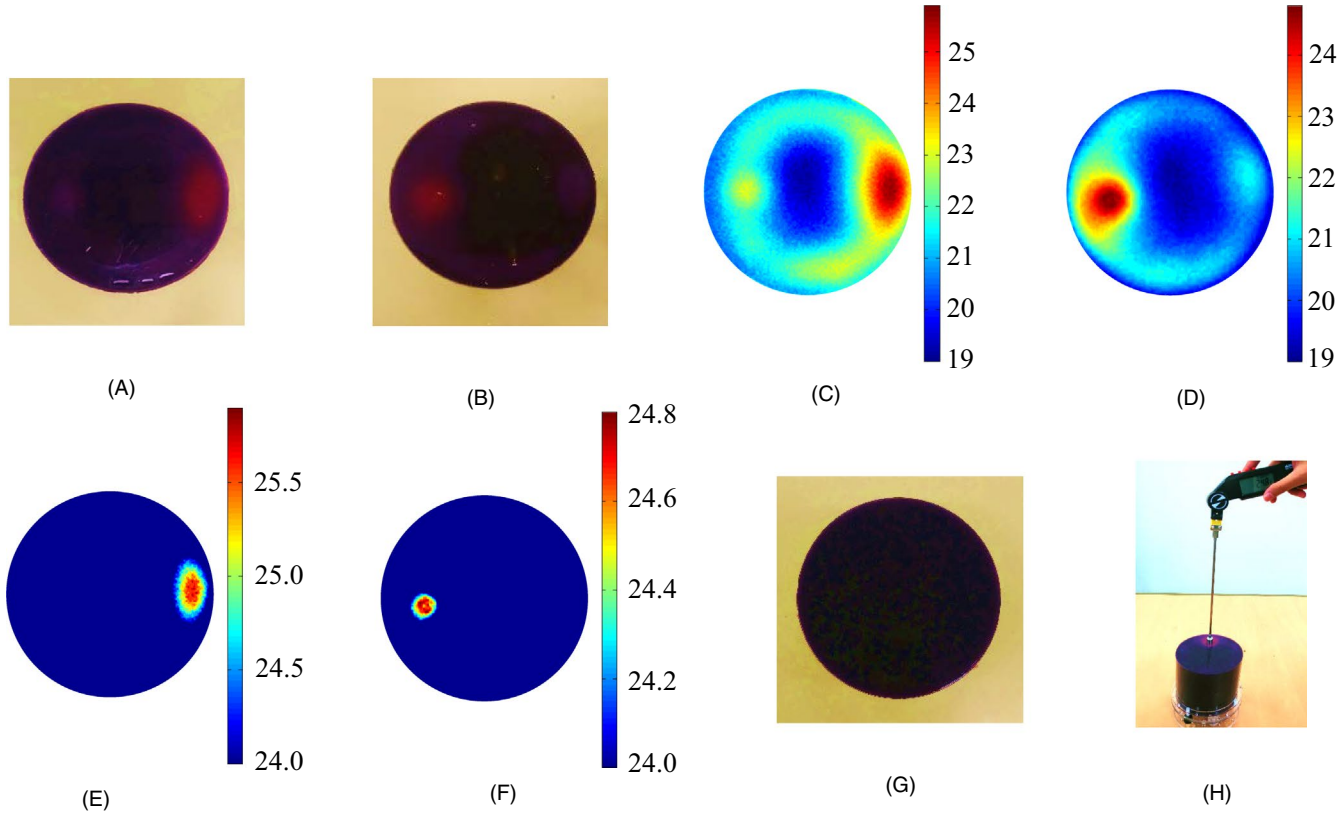

FIGURE 13 Experimental results of the beam focusing for the muscle-mimicking phantom using a threshold: (A) Experiment with a threshold of 1 and (B) experiment with a threshold of 0.3; the temperature measured at 10 min using (C) an IR camera with a threshold of 1 and (D) an IR camera with a threshold of 0.3; (E) a focal spot size with a threshold of 1 and (F) a focal spot size with a threshold of 0.3; using a thermometer with a threshold of 0.3 (G) before and (H) after the experiment

that the focal spot size of the phantom, as indicated in Figure 13A and 13C, applied with a threshold of 1, is 16 mm (x-axis) and 28 mm (y-axis) in the hot spot region of the right edge area when the reference temperature is 24 °C (relatively equal to 42 °C within a range of 37 °C–43 °C, at $= \Delta T$ 5 °C). As a result, the focal spot size in the hot spot region is smaller along the x-axis compared to the simulation result, and it is similar to the simulation result along the y-axis. This appears to be due to a measurement error in the experimental process and an error in the thermal properties of the muscle-mimicking phantom tissue. Figure 13F shows that the focal spot size of the phantom, as indicated in Figure 13B through 13D, applied with a threshold of 0.3, is 11 mm (x-axis, y-axis) corresponding to 0.25 λ_g at the target position when the reference temperature is 24 °C (relatively equal to 42 °C within a range of 37 °C–43 °C, where $= \Delta T$5 °C). Here, the experimental and simulation results of the focal spot size agree. Figure 13G shows an image corresponding to one of the two pieces of the truncated phantom prior to the experiment and compared to the experimental results. The experimental results agree with the simulation results described in Section IV. The experimental validation of the fabricated muscle-mimicking phantom does not indicate the occurrence of unwanted hot spots in the phantom, and beam focusing is effectively conducted at the target position of the phantom, as shown in Figure 13B. The simulation and experimental results of the proposed TR algorithm and the truncated threshold method prove the effectiveness of the beam focusing at the target position of the phantom while reducing unwanted hot spots in the surrounding normal tissue.

6 | CONCLUSIONS

A 3D beam focusing study for the noninvasive FMT of a muscle-mimicking phantom at 925 MHz was proposed. A truncated threshold method and a modified TR algorithm were proposed to reduce unwanted hot spots in the normal tissue region while a beam was appropriately focused at the target position of a phantom. We developed an FMT system and fabricated a muscle-mimicking phantom to validate simulation results. The simulation and experimental results confirmed that beam focusing is possible at the target position. The simulation results agreed with the experimental results, indicating that acceptable results can be achieved. In future studies, 3D simulation analysis will be conducted by utilizing a 3D anatomical model and animal experiments will be performed using the FMT system.

ACKNOWLEDGMENTS

This work was supported by an Electronics and Telecommunications Research Institute (ETRI) grant funded by the Korean government [18ZR1230, Research on Beam Focusing Algorithm for Microwave Treatment]. The authors thank ZMT for a donation until November 2017 of the Sim4Life tool used in this research.

REFERENCES

1. P. R. Stauffer, *Evolving technology for thermal therapy of cancer*, J. Hyperthermia **21** (2005), 731–744.
2. A. J. Fenn, *Adaptive phased array thermotherapy for cancer*, Artech House, Norwood, Massachusetts, 2009.
3. R. B. Roemer, *Engineering aspects of hyperthermia therapy*, Ann. Rev. Biomed. Eng. **1** (1999), 347–376.
4. M. Converse et al., *A computational study of ultra-wideband versus narrowband microwave hyperthermia for breast cancer treatment*, IEEE Trans. Microw. Theory Tech. **54** (2006), 2169–2180.
5. D. A. M. Iero et al., *Thermal and microwave constrained focusing for patient-specific breast cancer hyperthermia: A robustness assessment*, IEEE Trans. Antennas Propag. **62** (2014), 814–821.
6. J. Y. Kim et al., *Study of microwave energy localization in human tissue*, in Proc. IEEE AP-S Int. Symp. USNC/URSI National Radio Science Meeting, San Diego, USA, 2017, pp. 219–220.
7. B. J. Mohammed, A. M. Abbosh, and P. Sharpe, *Planar array of corrugated tapered slot antennas for ultrawideband biomedical microwave imaging system*, Int. J. RF Microw. Comput.-Aided Eng. **23** (2013), 59–66.
8. A. Dewantari et al., *Analysis of microwave-induced thermoacoustic signal generation using computer simulation*, J. Electromagn. Eng. Sci. **16** (2016), 1–6.
9. J. Y. Kim et al., *Computational study on focused microwave thermotherapy for knee pathological treatment*, IET Microw. Antennas Propag. **12** (2018), 1901–1907.
10. M. J. Burfeindt et al., *Microwave beamforming for non-invasive patient-specific hyperthermia treatment of pediatric brain cancer*, Phys. Med. Biol. **56** (2011), 2743–2754.
11. P. T. Nguyen, et al, *Three-dimensional microwave hyperthermia for breast cancer treatment in a realistic environment using particle swarm optimization*, IEEE Trans. Biomed. Eng. **64** (2016), 1335–1344.
12. A. T. Mobashsher, A. M. Abbosh, and Y. Wang, *Microwave system to detect traumatic brain injuries using compact unidirectional antenna and wideband transceiver with verification on realistic head phantom*, IEEE Trans. Microw. Theory Tech. **62** (2014), 1826–1836.
13. J. Stang et al., *A preclinical system prototype for focused microwave thermal therapy of the breast*, IEEE Trans. Biomed. Eng. **59** (2012), 2431–2438.
14. H. D. Trefná, J. Vrba, and M. Persson, *Time-reversal focusing in microwave hyperthermia for deep-seated tumors*, Phys. Med. Biol. **55** (2010), 2167–2185.
15. E. Zastrow, S. C. Hagness, and B. D. Van Veen, *3D computational study of non-invasive patient-specific microwave hyperthermia treatment of breast cancer*, Phys. Med. Biol. **55** (2010), 3611–3629.
16. Sim4life by ZMT, [Online]. Available: www.zurichmedtech.com.
17. M. Fink, *Time reversal of ultrasonic fields-part I: basic principles*, IEEE Trans. Ultrason. Ferroelectr. Freq. Control. **39** (1992), 555–566.
18. Z. Wang, J. Li, and R. Wu, *Time-delay-and time-reversal-based robust capon beamformers for ultrasound imaging*, IEEE Trans. Med. Imag. **24** (2005), 1308–1322.
19. X. Zhu et al., *Microwave-induced thermal acoustic tomography for breast tumor based on compressive sensing*, IEEE Trans. Biomed. Eng. **60** (2013), 1298–1307.
20. D. A. M. Iero et al., *Focusing time-harmonic scalar field in complex scenarios: A comparison*, IEEE Antennas Wireless Propag. Lett. **12** (2013), 1029–1032.
21. E. Zastrow et al., *Time-multiplexed beamforming for noninvasive microwave hyperthermia treatment*, IEEE Trans. Biomed. Eng. **58** (2011), 1574–1584.
22. M. E. Yavuz and F. L. Teixeira, *Frequency dispersion compensation in time reversal techniques for UWB electromagnetic waves*, IEEE Geosci. Remote Sens. Lett. **2** (2005), 233–237.
23. ITIS Foundation, Zurich, Switzerland, Available: www.Itis.ethz.ch.

AUTHOR BIOGRAPHIES

Jang-Yeol Kim received his BS and MS degrees in information and communication engineering from Chungbuk National University, Cheongju, Rep. of Korea, in 2010 and 2012, respectively, and his PhD in information and communication engineering from Chungbuk National University, in 2017. Since 2012, he has been with the Electronics Telecommunications Research Institute, Daejeon, Rep. of Korea. His research interests include antenna design, microwave sensing, thermal therapy algorithms, and electromagnetic sensors.

Kwang-Jae Lee received his BS and MS degrees in electronics, telecommunications, and computer engineering from Korea Aerospace University, Goyang, Rep. of Korea, in 2007 and 2010, respectively. Since 2010, he has been with the Electronics Telecommunications Research Institute, Daejeon, Rep. of Korea. His research interests include the design and analysis of electromagnetic structures, antennas, and bioelectronics systems.

Bo-Ra Kim received her BS and MS degrees in electronics, telecommunications, and computer engineering from Korea Aerospace University, Goyang, Rep. of Korea, in 2008 and 2009, respectively. From 2010 to 2019, she worked for the Electronics Telecommunications Research Institute, Daejeon, Rep. of Korea. Her research interests include microwave imaging and thermal therapy algorithms.

Soon-Ik Jeon received his BS and MS degrees in electronic engineering from Korea University, Seoul, Rep. of Korea, in 1984 and 1996, respectively, and his PhD in electronic engineering from Chungnam National University, Daejeon, Rep. of Korea, in 2003. From 1984 to 1990, he worked at Samsung Electronics, Seoul, Rep. of Korea, as a member of the research staff. Since 1990, he has been with the Radio Technology Research Department of the Electronics Telecommunications Research Institute, Daejeon, Rep. of Korea, as a principal member of the research staff. His current research interests include microwave applications and their systems for biomedical sensing and thermal therapy.

Seong-Ho Son received his BS degree in control and mechanical engineering from Pusan National University, Busan, Rep. of Korea, in 1997, and his MS and PhD degrees in mechanical engineering from Pohang University of Science and Technology, Pohang, Rep. of Korea, in 1999 and 2009, respectively. From 1999 to 2001, he worked for Daewoo Motors, Incheon, Rep. of Korea. From 2001 to 2019, he was a principal researcher with the Radio and Satellite Research Division of the Electronics Telecommunications Research Institute, Daejeon, Rep. of Korea. Since March 2019, he has been with the Department of Mechanical Engineering, Soonchunhyang University, Asan, Rep. of Korea, where he is working as an assistant professor. His main research interests include microwave sensing and imaging, medical thermal treatment, and radio mechatronics.